SAND2011-1989C

ILASS Americas, 23rd Annual Conference on Liquid Atomization and Spray Systems, Ventura, CA, May 2011

Many-body Dissipative Particle Dynamics simulation of capillary pinch-off

M. Arienti
Sandia National Laboratories
Livermore, CA 94550 USA

Abstract

The MDPD method provides a mesoscale description of the liquid-gas interface where molecules can be thought of as grouped in particles with modeled Brownian and dissipative effects. No liquid-gas interface is explicitly defined; surface properties, such as surface tension, result from the MDPD interaction parameters. In this paper, the mesoscale character of MDPD is demonstrated in the context of jet pinch-off by comparison with the asymptotic scaling predictions for large, intermediate and low Ohnesorge numbers. The predominant behavior at a large Oh number tends to be dominated by thermal fluctuations, whereas at smaller Oh a viscous-inertial and even an inviscid flow behavior can appear. One MDPD simulation in particular displays all the three regimes. The fact that the final stage leading to pinch-off is always stochastic – traditionally excluded in continuum discretizations – can have important consequences in spray modeling. This paper also shows how MDPD results can be assessed to be independent from the coarse-graining level. The thickness of the micro-bridge that forms just before capillary pinch-off is discussed in light of this convergence study. An example of modification of the jet pinch-off behavior due to the interaction with a still gas concludes this work.

Introduction

Continuum-scale hydrodynamic simulation has had rather impressive success in studying the behavior of fluids; nevertheless, there are still many problems for which such simulations have difficulties. In the study of free-surface flows, the advantage of methods like Dissipative Particle Dynamics (DPD) resides in the simplicity of the underlying algorithm of particle interaction under a soft repulsive potential.

While substantially less expensive than Molecular Dynamics (MD), DPD can be formally constructed from coarse-graining of Lennard-Jones clusters [1]. DPD has been used to investigate phase separation in immiscible binary liquid mixtures [2], [3] [4], droplet deformation and rupture in shear flow [5], and droplets on surfaces under the influence of shear flow [6]. The standard DPD method presents, however, a fundamental limitation, in that the repulsive soft potential alone cannot reproduce surface tension in single-species fluid flows. The DPD potential leads to a predominantly quadratic pressure-density equation of state (EOS) [7], while a higher-order pressure-density curve is necessary for the coexistence of the liquid and vapor phases.

Single-species phase coexistence in a liquid occurs in the range of densities $\rho_V < \rho < \rho_L$ where ρ_V and ρ_L are the pure vapor and liquid number densities. In that state, surface tension emerges from the asymmetry of the intermolecular forces acting on a layer of molecules at the liquid-vapor interface. As this asymmetry causes larger intermolecular distances in the outer layer than in the liquid bulk, the forces in the layer act to contract the interface.

The Many-body DPD (MDPD) method by Pagonabarraga and Frenkel [8] adds an attractive force to DPD. The amplitude of the soft repulsion is made proportional to the local density of the particles, thus achieving a cubic pressure-density relation. A similar approach has been introduced by Nugent and Posch in the context of Smoothed Particle Hydrodynamics (SPH) [9]. The MDPD method was also extensively investigated by Warren [10] and Trofimov et al. [11]. The dependence of surface tension on the interaction parameters and the relation with the bulk density of the fluid were explored by Arienti et al. [12].

In this paper, the MDPD technique is applied to the study of liquid thread pinch-off. After outlining the workings of MDPD, an example illustrates the link between the interaction forces and the fluid properties. The sense in which an MDPD simulation can converge to a time-dependent solution is also explained is this introductory section. The main body of the paper demonstrates the ability of MDPD to capture the complete sequence of scaling behavior – inviscid, inertial-viscous and stochastically dominated – that asymptotic analysis has identified. Simulations are carried out for different viscosities of the fluid and in the presence of a DPD gas.

MDPD scheme

MDPD inherits the three pairwise-additive inter-particle forces formulation of the standard DPD scheme. The conservative, dissipative and random forces are defined, respectively, as

$$\mathbf{F}_{ij}^{C} = F_{ij}^{C}(r_{ij})\hat{\mathbf{r}}_{ij} \tag{1}$$

$$\mathbf{F}_{ij}^{D} = -\omega_D(r_{ij})(\mathbf{v}_{ij}\cdot\hat{\mathbf{r}}_{ij})\hat{\mathbf{r}}_{ij} \tag{2}$$

$$\mathbf{F}_{ij}^{R} = -\xi\omega_R(r_{ij})\hat{\mathbf{r}}_{ij} \tag{3}$$

where $\hat{\mathbf{r}}_{ij} = \mathbf{r}_{ij}/r_{ij}$ and $\mathbf{v}_{ij} = \mathbf{v}_i - \mathbf{v}_j$.

Warren's approach [13] is pursued for the conservative term. The repulsive force depends on a weighted average of the local density, whereas the attractive force is density-independent:

$$\mathbf{F}_{ij}^{C} = A_{ij}\omega_c(r_{ij}) + B_{ij}(\overline{\rho}_i + \overline{\rho}_j)\omega_d(r_{ij}) \tag{4}$$

The weight functions $\omega_c(r) = (1 - r/r_c)$ and $\omega_d(r) = (1 - r/r_d)$ vanish for $r > r_c$ and $r > r_d$,

respectively. Since a DPD method with a single range may not have a stable interface [9], in Equation (4) the repulsive contribution is set to act at a shorter range $r_d < r_c$ than the soft pair attractive potential. The many-body repulsion is chosen in the form of a self-energy per particle which is quadratic in the local density, $B_{ij}(\overline{\rho}_i + \overline{\rho}_j)\omega_d(r_{ij})$, where $B > 0$. The density for each particle is defined as

$$\overline{\rho}_i = \sum_{j \neq i} \omega_\rho(r_{ij}) \tag{5}$$

and its weight function ω_ρ is defined as

$$\omega_\rho(r) = \frac{15}{2\pi r_d^3}(1 - r/r_d)^2. \tag{6}$$

The kernel vanishes for $r > r_d$ and for convenience it is normalized: $\int d^3\mathbf{r}\,\omega_\rho(r) = 1$.

The DPD thermostat consists of random and dissipative forces, which maintain the equilibrium temperature T through the condition posed by the fluctuation-dissipation theorem

$$\xi^2 = 2\gamma k_B T, \tag{8}$$

where k_B is the Boltzmann constant. The weight function for the dissipative force is

$$\omega_D(r) = (1 - r/r_c)^2 \tag{9}$$

Details about the choice of ξ and γ can be found in [13]. The simulations presented in this work are carried out with the velocity Verlet algorithm of Groot and Warren [13] using the empirical parameter value of 1/2.

Since the random and dissipative forces of MDPD are common with DPD, particles from the two schemes can be easily combined. This enables the simulation of more complex flows, for instance the inclusion of a surrounding gas taking part to pinch-off. Table 1 offers an example of two different sets of parameters: the first row corresponds to an MDPD fluid, the second to a DPD gas. In the latter, the sign of the coefficient A is switched and there is no density-dependent term. An example of MDPD-DPD interaction will be presented later.

We conclude this Section by mentioning that the simulations enabled by the particle dynamics software code LAMMPS (Large-scale Atomic/Molecular Massively Parallel Simulator) [14] with the addition of a new MDPD class. The computationally scalable implementation of LAMMPS guarantees the optimization of the interaction calculation through an efficient neighbor list algorithm, and will not be discussed here.

MDPD properties

Conventionally, dissipative particle dynamics methods operate in reduced units, so that length is measured in units of r_c and mass in units of m, the mass of a single particle. The behavior of a MDPD system can then be captured by choosing the physical units of length (L_{DPD}), mass (M_{DPD}), and time (T_{DPD}). This becomes relevant if one wants to obtain a specific set of MDPD properties, for instance in relation with the properties of a real liquid.

Let us consider the set of interaction parameters A = -40, B = 25, r_d = 0.75, see Table 1. The number density ρ, kinematic viscosity ν and the surface tension coefficient σ are not simulation inputs, but they can be evaluated with simple numerical tests. By applying the Young-Laplace relation to a spherical drop in equilibrium we find ρ = 6.1 and σ = 7.3; see Ref. [12] for a systematic study of the dependence of surface tension on the interaction parameters. Viscosity can be assessed in a test where a doubly periodic Poiseuille (DPP) flow is established; the description of a convenient procedure for creating two opposite Poiseuille flows can be found in Ref. [15]. In this example, the kinematic viscosity is determined by γ = 0.005 and ξ = 0.1.

If the same properties of surface tension coefficient, density and viscosity are expressed in physical units and labeled with an asterisk, dimensional analysis yields to

$$M_{DPD} = L_{DPD}^3 \frac{d_*}{d}$$
$$T_{DPD} = \left(M_{DPD} \frac{\sigma}{\sigma^*} \right)^{1/2} \qquad (10)$$
$$\frac{L_{DPD}^2}{T_{DPD}} = \frac{\nu^*}{\nu}$$

From these equations, the properties of water at ambient conditions (d^* = 998 kg/m^3, σ^* = 0.0720 N/m, and ν^* = 1.00 · 10^{-6} m/s^2) are matched by taking M_{DPD} = 3.94 · 10^{-18} kg, T_{DPD} = 7.32 · 10^{-7} s, and L_{DPD} = 3.18 ·10^{-6} m. The number of molecules per MDPD particle can now be obtained directly from M_{DPD} divided by the mass of a water molecule; it is n = 1.47 · 10^7. The set of equations (10) reveals the link between the viscosity of the system and L_{DPD}: everything else being the same, the smaller is ν^*, the greater is the coarse graining.

It is to be noted that other properties, such as the non-dimensional isothermal compressibility $\kappa^{-1} = (\partial P/\partial \rho)_T / k_B T$, do not generally coincide with the properties of water. For this MDPD fluid, we find $\kappa^{-1} \approx 50$ (based on the generalized equation of state proposed by Warren [10]), whereas the actual value for water κ^{-1} = 16. Thus, the operation of matching surface tension coefficient, density and kinematic viscosity of a liquid may lead to different interaction parameters than the ones obtained by imposing equal compressibility.

We close this section by noting that the MDPD kinematic viscosity can be decreased by reducing γ, as shown on Table 2. This operation can be carried out while keeping the temperature of the fluid the same, as long as ξ is varied according to Equation (8). Of the values listed on Table 2, the viscosity γ = 288 was calculated for the DPD parameters A = 10, B = 0, r_d = 0, and with particle mass m = 0.00647; see the bottom row on Table 1. At these conditions, the number density is of ρ_G = 0.935 particles per unit cube and the compressibility is $\kappa^{-1} \approx 1 + 0.202\,\rho_G / k_B T$ = 1.19.

Table 1. Example of parameter sets for DPD and MDPD fluids.

m	A	r_c	B	r_d
1	-40	1	25	0.75
0.00647	10	1	0	0

Table 2. Kinematic viscosity of DPD and MDPD fluids at $k_B T$ = 1.

γ	2	72	0.5	0.005
ν	0.96	2.8	0.93	0.072

MDPD coarse-graining

MDPD is proposed as a truly mesoscopic method that can bridge the gap between the atomistic scale (in the range of nanometers and nanoseconds) that is accessible by molecular dynamics (MD) simulations and the macroscopic scale (in the range of micrometers and milliseconds) considered by continuum descriptions. To this end, it is important to define in what sense the method is scalable.

Let us consider a system whose particle number N has been scaled by a factor ϕ while keeping the domain size constant. Denoting with a prime the new equivalent system, so that $N' = N/\phi$ and $m' = m\,\phi$, the scaling relations in three dimensions are $r_c' = r_c\,\phi^{1/3}$ and $t' = t\,\phi^{1/3}$. The first relation maintains the fractional particle overlap in the change of the coarse-graining level, while the second ensures that velocity increments calculated during one time step are the same for the two systems. The approach proposed by Füchslin [16] for DPD requires the modification of the interaction parameters as a function of the coarse-graining level. For the same argument, the scaled force parameters are

$$A' = A\,\phi^{2/3} \qquad (11)$$
$$\gamma' = \gamma\,\phi^{2/3} \qquad (12)$$

$$\xi' = \xi\,\phi^{2/3} . \qquad (13)$$

This procedure can be extended to MDPD by adding the primed parameters [12]

$$r_d' = r_d\,\phi^{1/3} \qquad (14)$$

$$B' = B\,\phi^{5/3} . \qquad (15)$$

From the relations above, scale independence holds for bulk interactions because the energy associated with an individual MDPD particle is made proportional to the number of molecules it represents. It is noted, however, that, while the stress tensor terms are unaffected by coarse-graining, the kinematic viscosity scales like $\phi^{1/3}$. Thus, for an increased coarse-graining $N'/N > 1$ (so that $\phi < 1$), the viscosity, $\nu' = \nu\,\phi^{1/3}$, decreases. Similarly, even if $\sigma' = \sigma\,\phi^{1/3}$, the surface tension is invariant ($\phi^{1-1/3-2/3} = \phi^0$).

Coarse-graining is illustrated in Figure 1, with the same calculation repeated for $\phi = 1/8$ in frame (b), $\phi = 1/64$ in frame (c), and $\phi = 1/512$ in frame (d). Details of the numerical setting of the simulation will be explained later; for the moment it suffices to say that snapshots show a slice of a liquid jet immediately after pinch-off. The simulation in frame (a) includes 287 particles and takes less than a minute to run on a single-core CPU. The number of particles increases by a factor 8 in each following calculations, while the interaction parameters correspondingly decrease according to Equations (11) to (15).

The jet, repeated periodically in the axial direction, is 10 DPD units long. This length corresponds to 31.8 μm in the physical units from the previous section. The initial diameter is 7.07 μm. As coarse graining is reduced, the development of a thin liquid bridge that rapidly retreats toward the newly formed drops becomes more defined. The shape of the pinched thread converges at $\phi = 1/64$.

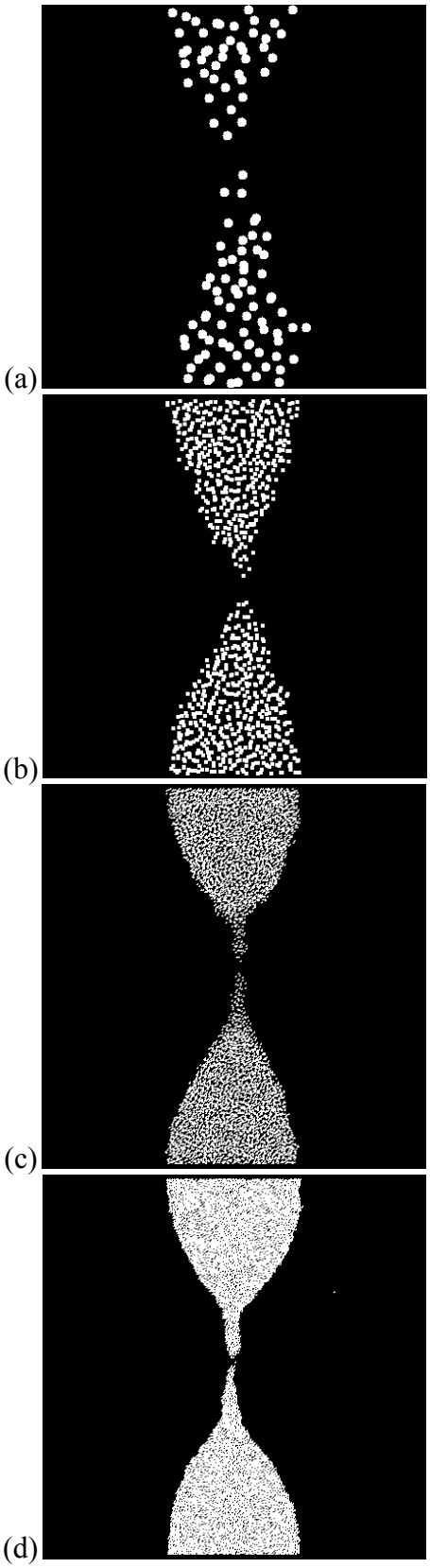

Figure 1. Convergence study of jet pinch-off. See text for details.

Overall, no qualitative differences between the different levels of coarse-graining; particularly, no satellite drops are observed for this configuration. A second series of calculations at a larger jet radius (not shown here) confirms that the Plateau condition on the minimum surface energy for pinch-off is respected independently from coarse-graining: the jet returns to the equilibrium cylindrical shape if the jet radius R is larger than $\lambda/2\pi$, where λ is the wavelength of the axial perturbation.

Local dynamics near pinch-off

A number of authors have carried out local analyses of the Navier–Stokes, Stokes and Laplace equations for pinching threads; see, for instance, the extensive review in Ref [18]. To establish a connection with the theory, the minimum thread radius h_{min} from an MDPD simulation is plotted in this Section as a function of the time to breakup, τ. It is expected that $h_{min}(\tau)$ follows a specific power law depending on the Ohnesorge number, $\mathrm{Oh} = \rho^{1/2}\nu / (R\sigma)^{1/2}$, even if in reality every MDPD simulation has its own specific trajectory.

In the absence of an outer fluid, breakup asymptotically proceeds according to a solution that balances surface tension, viscous, and inertial forces. However, for sufficiently small values of Oh, viscosity must drop out of the description; taking the characteristic length scale to be the minimum radius, it follows from dimensional analysis that $h_{min} \sim (\sigma\tau^2/\rho)^{1/3}$. Viscous effects eventually become important as the minimum radius continues to decrease and becomes of order Oh^2. At that point the flow then transitions to an inertial-viscous scaling regime, where $h_{min} \sim \tau$.

On even smaller scales, it can be postulated that the driving force leading to pinch-off consists of thermal fluctuations at the molecular level. The relevant length scale appears from the comparison of the thermal energy with the surface energy,

$$\ell_T = \sqrt{k_B T/\sigma}\,. \qquad (16)$$

The domain concerned by thermal fluctuations (up to a few hundreds of nanometers) has been probed only recently by Molecular Dynamics simulations of nanojets [19]. A set of one-dimensional dynamical equations can also be derived from the Navier-Stokes equations in the limit of a thin layer of liquid where inertia, the component of velocity normal to the surface, and the in-plane derivatives are neglected. These "lubrication equations" are fully deterministic, but stress fluctuations can be added via a stochastic term [21]. The flow obeying to the Stochastic Lubrication Equations exhibits a characteristic self-similar profile resembling two cones joined at their apexes (called the double-cone profile) and leading to a symmetric pinch-off. The relation between h_{min} and τ is described by a power law with exponent 0.418 [20].

According to theory then, it should be possible to observe in a logarithmic plot of $h_{min}(\tau)$, the 2/3 slope first, then the slope 1, and finally the 0.418 slope. However, spanning the three scaling behaviors in a single pinch-off simulation has so far proven prohibitive from a computational point of view. As mentioned earlier, the first transition from inviscid behavior depends on Oh, but the second occurs for $h_{min} \sim \mathrm{Oh}^2$, at sub-micron scales for most liquids. In the following example we will demonstrate that such a simulation is possible with MDPD. To this end, instead of changing the domain scale, we take a constant reference jet radius, as well as given fixed values of surface tension and density and modify the viscosity.

The effect of viscosity on the shape of the jet near pinch-off is shown in Figure 2 for two cases at low and high viscosity. A small axial perturbation is applied to the jet with wavelength $\lambda = 40$. The jet radius is chosen so that $\lambda/R = 9.01$. This length-to-radius ratio corresponds to the fastest growing rate of capillary instability according to linear analysis.

In the low-viscosity case, with $\nu = 0.072$, the extended thin long thread before pinch-off is in agreement with the deterministic approximation to the Navier-Stokes equations. It can be shown that this profile is in fact a universal solution (i.e., independent of initial conditions) of the deterministic lubrication equations. The high viscosity case, with $\nu = 2.8$, is instead closer to the double-cone self-similar profile of the Stochastic Lubrication Equations [21]. This shape is typically observed in MD simulations of nanojets [19].

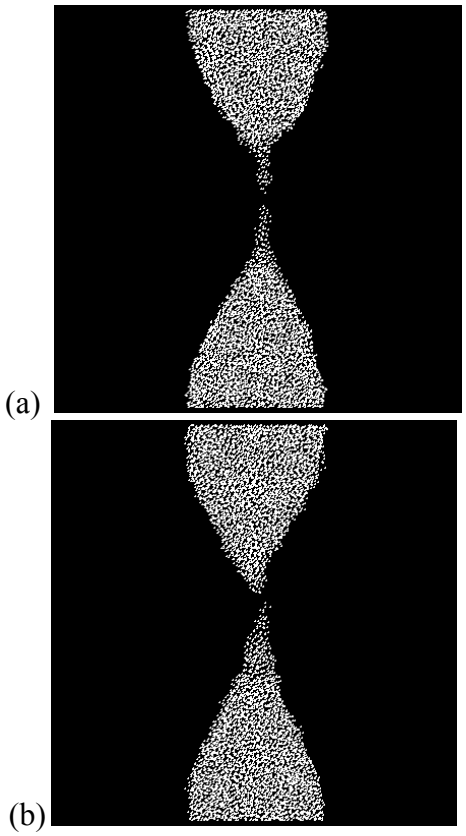

Figure 2. Effect of increasing viscosity on pinch-off: (a) $\nu = 0.072$; (b) $\nu = 2.8$.

A more quantitative analysis is provided by the logarithmic behavior of $h_{min}(\tau)$. To track the minimum jet radius as a function of time, it is necessary to post-process several snapshots of particles position according to the following procedure. The computational domain is first axially divided into 50 bins; then the center of mass of each slice of the jet is calculated. This is a crucial step in measuring the radius profile because the liquid thread can oscillate during the pinch-off process. For each bin, a number density histogram is constructed in annular rings with a radial increment of 10^{-3} units. Finally, the surface of the liquid slice is identified at a position such that 1% or less of the particles of the bin lie outside the surface. This small number of particles is assumed to belong to the vapor phase – a threshold consistent with a simulation with almost no vapor phase. For each simulation, the pinch-off time is established as the instant when one of the bins becomes empty. The time to pinch-off τ is normalized by the capillary time scale $(\rho R^3/\sigma)^{1/2}$, whereas h_{min} is normalized by R.

The log-log plot of $h_{min}(\tau)$ in Figure 3 corresponds to the largest viscosity $\nu = 2.8$. It shows a noise-dominated behavior where most of the tracked points are aligned along the slope 0.418. At a smaller value of viscosity, $\nu = 0.93$, the inertial-viscous slope 1 begins to appear (Figure 3); the transition to stochastic behavior is roughly located at $h_{min}/R \sim 0.1$. At an even smaller viscosity, $\nu = 0.072$, the 2/3 power inviscid scaling also appears, albeit briefly (Figure 5). The transition from inviscid to viscous-inertial takes place at $h_{min}/R \sim 1$, whereas the transition to stochastic remains at $h_{min}/R \sim 1$.

From a practical point of view, this set of MDPD simulations suggests that, for a liquid with the properties of water, stochastic effects begin to appear when the liquid thread reaches a radius of 0.1 R, corresponding to 1.2 μm. Equation (16) also gives $\ell_T = 0.37$ DPD units, that is, $\ell_T = 1.2$ μm.

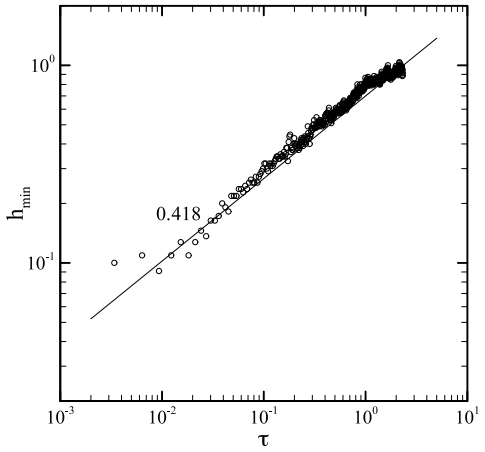

Figure 3. Variation of h_{min} with τ when Oh = 1.2. ($\nu = 2.8$).

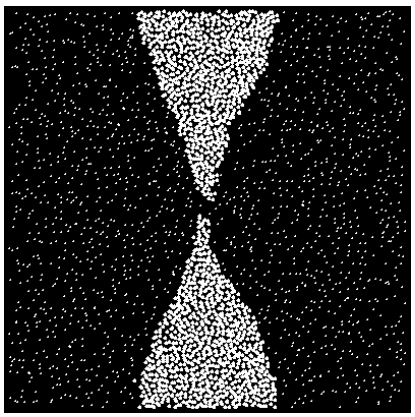

Figure 6. MDPD fluid pinch-off in a still DPD gas.

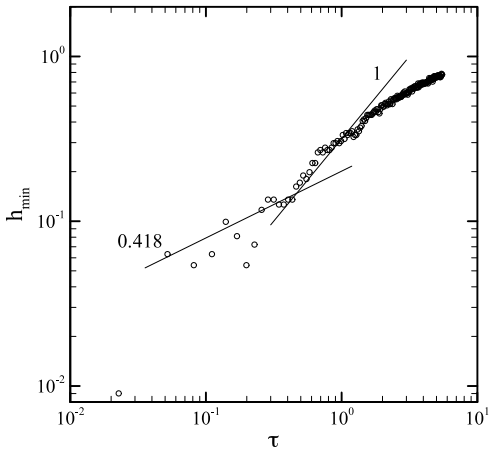

Figure 4. Variation of h_{min} with τ when Oh = 0.40 ($\nu = 0.93$).

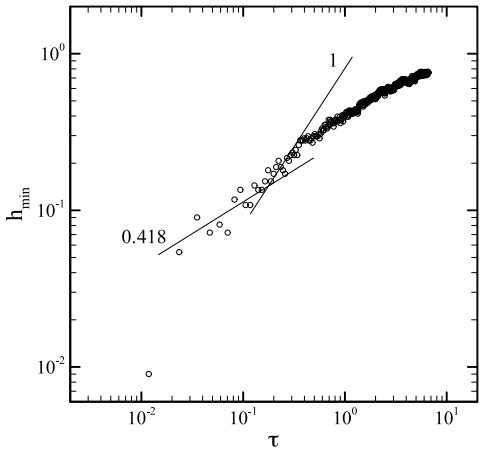

Figure 7. Variation of h_{min} with τ when Oh = 0.031 in the presence of a DPD gas ($\nu_G / \nu_L = 13$).

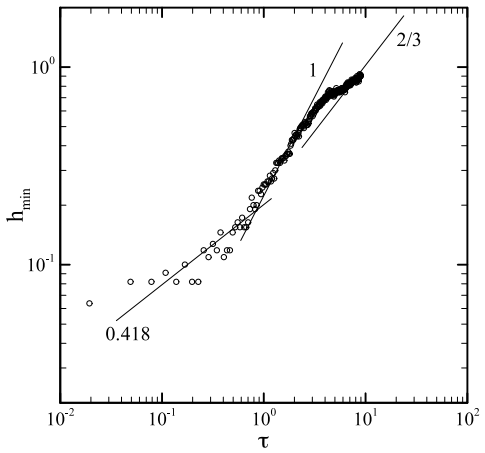

Figure 5. Variation of h_{min} with τ when Oh = 0.031 ($\nu = 0.072$).

The effect of the ambient gas on the dynamics of pinch-off can be neglected until $h_{min} \sim M\,\mathrm{Oh}^2$, where M is the ratio of the viscosity of the ambient gas to that of the liquid. We add now a DPD gas with the parameters listed on Table 1, bottom row. The values are selected to obtain the density ratios of water with respect to air: $(m\rho)_G / (m\rho)_L = 998$. The dissipation parameters are set so that $\nu_G / \nu_L = 13$. The inter-particle DPD-MDPD parameters are the same as the DPD parameters: $A = 10$, $r_c = 1$, $B = 0$, $r_d = 0$, $\gamma = 2$ and $\xi = 2$. The repulsive force coefficient between the liquid and the gas is the smaller possible value to avoid inter-penetration of the two species, but

no studies are presently available to define what the correct values should be.

A snapshot of the simulation is shown in Figure 6 whereas $h_{min}(\tau)$ in shown in Figure 7. Both plots indicate that the effective behavior of the MDPD fluid is more viscous in the presence of a still gas even if the Oh number is small.

Conclusions

The spatial and temporal meso-scales (within 10 and 1000 nm, and within 1 ns and 10 ms) that are captured by coarse-graining particle techniques can significantly extend the reach of molecular dynamics (MD) simulations while keeping the fundamental viewpoint that fluid properties arise from elementary particle interactions. In particular, the MDPD scheme provides a viable mesoscale description of free-surface flow.

This papers shows how matching the surface tension coefficient, the density and the kinematic viscosity of a given liquid with the properties of a system of MDPD particles determines all the interaction parameters. In a convergence study applied to jet pinch-off, the occurrence and shape of a thin liquid thread are shown to be independent from the level of coarse-graining.

MDPD simulations also agree with asymptotic scaling predictions at large, intermediate and low Oh number. The predominant behavior at large Oh is more dominated by thermal fluctuations, whereas at smaller Oh a viscous-inertial and even an inviscid flow behavior can appear. One simulation in particular displays all three regimes, proving the truly mesoscopic range of MDPD.

A simple demonstration of a two-species flow concludes this work. It is in fact natural to use MDPD to model a liquid and DPD to model a gas, since both techniques use the same thermostat. Future work will concentrate on imposing a flow rate on the gas field, so that pinch-off under shear can be simulated.

Acknowledgements

This work was partially supported by the AFOSR contract AFD-070820-034 under the supervision of Dr. Fariba Fahroo.

References

1. H. Lei, B. Caswell, and G. E. Karniadakis. Direct construction of mesoscopic models from microscopic simulations. Physical Review E, 81(4):026704:1–10, 2010.
2. P. V. Coveney and K. E. Novik. Computer simulations of domain growth and phase separation in two-dimensional binary immiscible fluids using dissipative particle dynamics. Physical Review E, 54:5134, 1996.
3. S. I. Jury, P. Bladon, S. Krishna, and M. E. Cates. Test of dynamical scaling in three-dimensional spinodal decomposition. Physical Review E, 59:R2535, 1999.
4. K. E. Novik and P. V. Coveney. Spinodal decomposition of off-critical quenches with a viscous phase using dissipative particle dynamics in two and three spatial dimensions. Physical Review E, 61:435–448, 2000.
5. A. T. Clark, M. Lal, J. N. Ruddock, and P. B. Warren. Mesoscopic simulation of drops in gravitational and shear fields. Langmuir, 16:6342– 6350, 2000.
6. A. A. Louis, P. G. Bolhuis, and J. P. Hansen. Mean field fluid behavior of the gaussian core model. Physical Review E, 62:7961–7972, 2000.
7. J. L. Jones, M. Lal, J. N. Ruddock, and N. Spenley. Dynamics of a drop at a liquid/solid interface in simple shear fields: a mesoscopic simulation study. Faraday Discuss., 112:129–142, 1999.
8. I. Pagonabarraga and D. Frenkel. Dissipative particle dynamics for inter- acting systems. Journal of Chemical Physics, 115(11):5015–5026, 2001.
9. S. Nugent and H. A. Posch. Liquid drops and surface tension with smoothed particle

applied mechanics. Physical Review E, 62:4968–4975, 2000.
10. P. B. Warren. Vapor-liquid coexistence in many-body dissipative particle dynamics. Physical Review E, 68:066702, 2003.
11. S. Y. Trofimov, E. L. F. Nies, and M. A. J. Michels. Constant-pressure simulations with dissipative particle dynamics. Journal of Chemical Physics, 123(14):144102, 2005.
12. M. Arienti, W. Pan, X. Li, and G. Karniadakis. Many-body Dissipative Particle Dynamics simulation of liquid/vapor and liquid/solid interactions. Submitted to the Journal of Chemical Physics.
13. R. D. Groot and P. B. Warren. Dissipative particle dynamics: bridging the gap between atomistic and mesoscopic simulation. Journal of Chemical Physics, 107:11:4423–4435, 1997.
14. S. J. Plimpton. Fast parallel algorithms for short-range molecular dynamics. Journal of Computational Physics, 117(1):1–19, 1995.
15. D. C. Visser, H. C. J. Hoefsloot, and P. D. Iedema. Modelling multi-viscosity systems with dissipative particle dynamics. Journal of Computational Physics, 214:491–504, 2006.
16. R. M. Füchslin, H. Fellerman, A. Eriksson, and H-J Ziock. Coarse graining and scaling in dissipative particle dynamics. Journal of Chemical Physics, 130:214102:1–8, 2009.
17. J. Eggers. Universal pinching of 3d axisymmetric free-surface flow. Phys. Rev. Lett. 71, 3458–3460, 1993.
18. R. F. Day, E. J. Hinch, and J.R. Lister. Self-similar capillary pinch-off of an inviscid fluid. Phys. Rev. Lett. 80, 704–707, 1998.
19. W. Kang. Molecular dynamics simulations and microscopic hydrodynamics of nanoscale liquid structures, Ph.D. thesis, Georgia Institute of Technology, 2008.
20. J. Eggers, Dynamics of liquid nanojets. Phys. Rev. Lett. 89, 084502, 2002.
21. M. Moseler and U. Landman. Formation, Stability, and Breakup of Nanojets. Science 289, 1165, 2000.